Supporting Information

Programmable Soft Valves for Digital and Analog Control

Colter J. Decker, Haihui Joy Jiang, Markus P. Nemitz, Samuel E. Root, Anoop Rajappan, Jonathan T. Alvarez, Jovanna Tracz, Lukas Wille, Daniel J. Preston, and George M. Whitesides

C.J. Decker, Dr. H.J. Jiang, Dr. S.E. Root, J. Tracz, L. Wille, Prof. G.M. Whitesides*
Department of Chemistry and Chemical Biology, Harvard University, 12 Oxford Street, Cambridge, MA 02138, USA
E-mail: gwhitesides@gmwgroup.harvard.edu

C.J. Decker, Dr. A. Rajappan, Prof. D.J. Preston*
Department of Mechanical Engineering, Rice University, 6100 Main Street, Houston, TX 77005, USA
E-mail: djp@rice.edu

Prof. M.P. Nemitz
Department of Robotics Engineering, Worcester Polytechnic Institute, 85 Prescott Street, Worcester, MA 01609, USA

J.T. Alvarez
John A. Paulson School of Engineering and Applied Sciences, Harvard University, 29 Oxford Street, Cambridge, MA 02138, USA

1. Rolling Diaphragm Piston Fabrication

Each piston actuator in this work is assembled from three components: a flexible thermoplastic polyurethane (TPU) rolling diaphragm and two compliant polypropylene piston chambers (i.e., sections of a drinking straw) of different diameters. To fabricate the diaphragm (**Figure S1**a-b), two layers of TPU (Stretchlon 200, Airtech International Inc.) were heat pressed on either side of a non-bonding layer of parchment paper (Heavy Duty Parchment, Katbite). This non-bonding layer is cut at 30% power and 70% speed using a laser cutter (14000 Laser System, Epilog). The vector graphics file used for laser cutting is given in Data File S1. The heat press (DK20SP, Geo Knight and Co Inc.) bonds the TPU layers to each other at 145 ℃ and 60 psi for 30 seconds. After pressing, the diaphragms were cut out from the surrounding TPU. The non-bonding layer was manually removed (Figure S1c).

The piston chamber consists of a 5 cm length of wide polypropylene straw (ST12100-Clear, Alink) connected to a silicone input tube (5054K321, McMaster-Carr) using two diameters of heat shrink tubing (6363K213, McMaster-Carr) and (6363K214, McMaster-Carr). After aligning the components (Figure S1d), the heat shrink is activated with a heat gun (SDL-8622, Yome) on the low setting (Figure S1e). The piston is then assembled by taping the diaphragm (Figure S1f) to the outside of the piston chamber with tape (Matte Finish Magic Tape, Scotch). If the piston will function independently, a plain, unmodified drinking straw (HS-1711272052, Hulless) is inserted as the piston rod. Alternatively, if the piston is a component in another device (i.e., a valve, SR latch, or regulator), the piston rod functions as an interface and is fabricated and added later. See Movie S1 for a demonstration of this fabrication process.

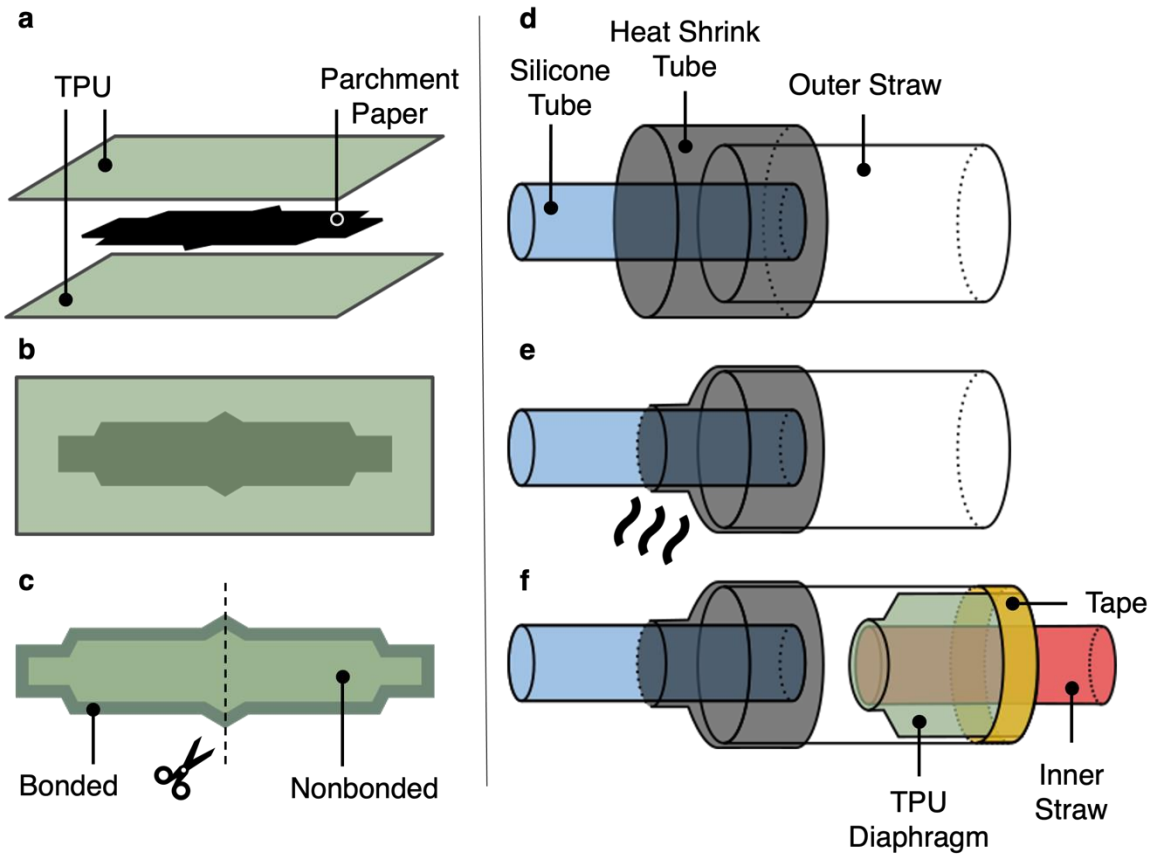

Figure S1. Rolling diaphragm piston fabrication. (a-b) Side and top view of TPU and parchment paper alignment before heat pressing. (c) Complete diaphragm after heat press. (d) Alignment of input tube, heat shrink tubing, and outer straw. (e) Piston chamber after applying heat. (f) Completed rolling diaphragm piston.

2. Pneumatic Switch Fabrication

The pneumatic switch consists of two laser-patterned straws and silicone tubing (51135K11, McMaster-Carr). The inner drinking straw (HS-1711272052, Hulless) is laser cut (14000 Laser System, Epilog) at 10% speed and 30% power with four holes for the silicone tubing (**Figure S2**a). The outer straw (ST12100-Clear, Alink) is laser cut at 30% speed and 70% power with two offset slits for tubing to pass through (Figure S2c). To assemble the switch, silicone tubing (51135K11, McMaster-Carr) is fed through each pair of holes (Figure S2b) and secured with a fast-drying glue (45198, Loctite). The inner straw and tubing are inserted into the outer straw and diagonally opposite tubes are secured with tape (Matte Finish Magic Tape, Scotch) and glue (45198, Loctite), as shown in Figure S2d. We leave 14 mm of tubing between the inner straw and the edge of the offset slit where the tubing is secured.

Minor modifications to this fabrication process are necessary if the switch is used as a component in another device (valve, regulator, or SR latch). These modifications are described below. Note that Figure S2 depicts a switch intended for use in a valve.

Switch for Valve: A second set of smaller holes are laser cut into inner piston rod at a 90-degree angle with respect to the holes intended for silicone tubing (Figure S2a). This second set of holes is connected with a slit to which up to four rubber bands (12205T75, McMaster-Carr) can be connected. Two additional slits are also laser cut on the outer straw chamber, through which the rubber bands may pass. Finally, two notches are laser cut on the end of the outer straw, allowing easy connection to a piston (Figure S2c). See Data File S2 and S3 for the laser files used while cutting the inner and outer straws for a valve, and Movie S1 for a demonstration of the fabrication process.

Switch for Regulator: The same modifications to a switch intended for a valve are also applied to a switch intended for a regulator. However, we use string instead of rubber bands in regulators (to directly transfer force to the piston head). Additionally, one of the silicone tubes (and associated holes) can be omitted to further simplify fabrication. See Data File S3 and S4 for laser files used while cutting the inner and outer straws of a regulator.

Switch for SR Latch: We laser cut four notches, two on each end of the outer switch chamber, to enable easy connection with pistons. See Data File S5 and S6 for laser files used while cutting the inner and outer straws of an SR latch.

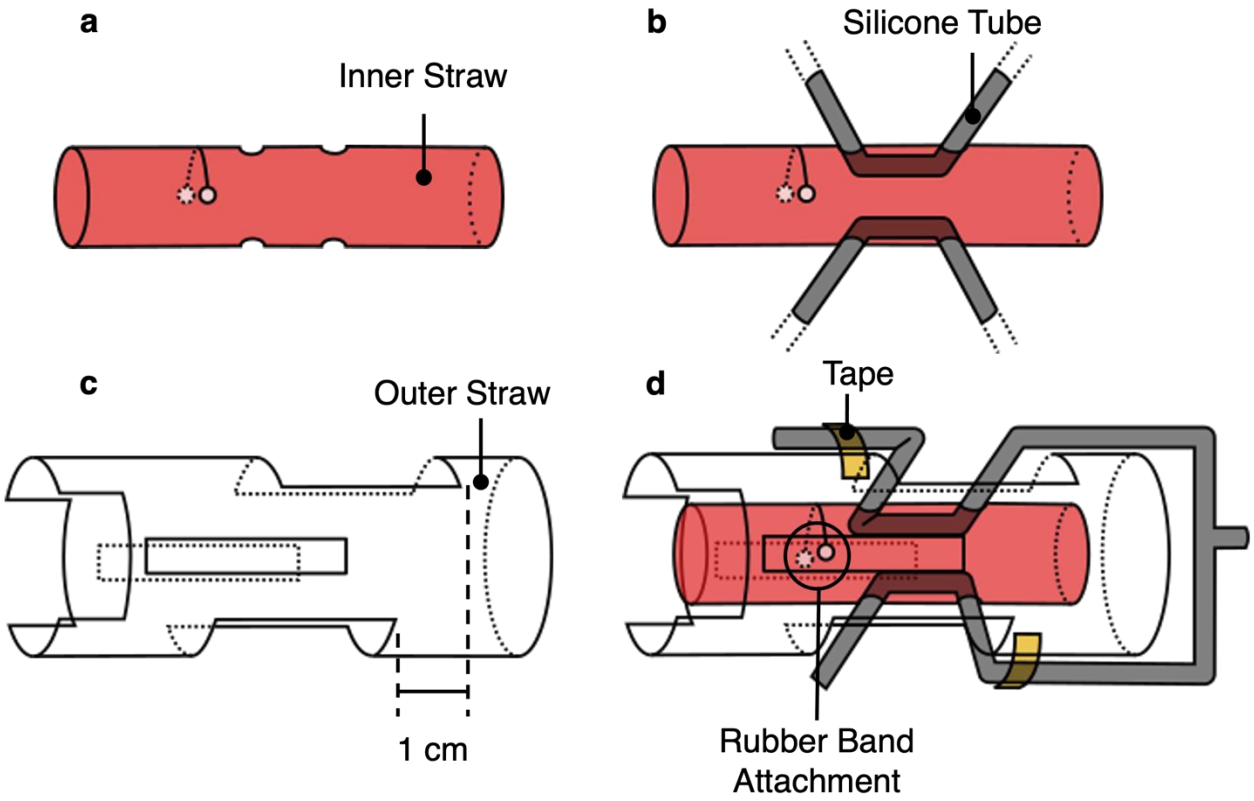

Figure S2. Pneumatic switch fabrication. (a) Laser-cut inner straw. (b) Inner straw with silicone tubing attached. Tubing is secured with superglue at the straw interface. (c) Laser cut outer straw. (d) Completed switch. Superglue is applied with tape to ensure attachment. In a completed valve, the rubber band will pull in parallel to the inner piston tube.

3. Valve Fabrication

Fabricating a valve requires a piston (with the inner straw omitted) and a switch (Figure S1-2). The piston is fastened to the switch using tape (Matte Finish Magic Tape, Scotch) as shown in **Figure S3**. Rubber bands (12205T75, McMaster-Carr) are attached through the laser cut holes and are restrained via attachment to the outer straw such that they are extended by 5 mm when the piston is unactuated. The material cost of one valve is approximately $0.40 (**Table S1)**.

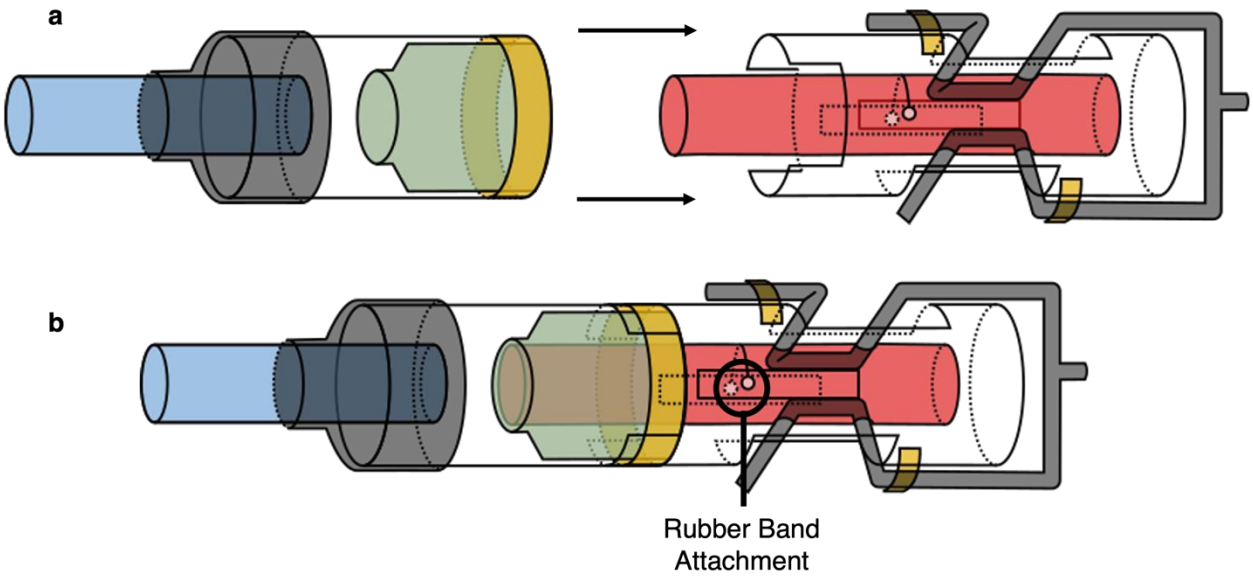

Figure S3. Valve fabrication. (a) Schematic of piston and switch before attachment. (b) Schematic of the completed valve. Materials are labeled in Figures S1-2.

Table S1. Estimated cost of materials (in USD) used for the fabrication of valves proposed in this work for digital and analog control

Description	Supplier	Amount	Unit	Cost	Amount/valve	Cost/valve
TPU	Airtech International Inc.	1.35	sqm	$3.50	0.002	$0.005
parchment paper	Katbite	247	sqm	$19.00	0.002	$0.000
PP straws, thick	Amazon	500	pcs	$10.00	0.30	$0.006
PP straws, thin	Amazon	500	pcs	$10.00	0.30	$0.006
silicone tube, thick	McMaster-Carr	0.30	m	$1.20	0.02	$0.080
silicone tube, thin	McMaster-Carr	0.30	m	$1.00	0.05	$0.167
heat shrink tube, thick	McMaster-Carr	3.0	m	$15.00	0.015	$0.075
heat shrink tube, thin	McMaster-Carr	3.0	m	$7.50	0.015	$0.038
rubber band	McMaster-Carr	1000	pcs	$10.00	1.0	$0.010
Krazy glue	Amazon	5	tubes	$8.00	0.005	$0.008
Scotch tape	Amazon	99	m	$14.00	0.04	$0.006
					Total cost / valve	**$0.40**

4. Regulator Fabrication

Fabricating a regulator requires a piston and switch (Figures S1-2). The piston is fastened to the switch with tape (Matte Finish Magic Tape, Scotch) as shown in **Figure S4**. A restraint (elastic band or string) is attached to the outer straw (thereby putting horizontal tension on the inner piston), and the pneumatic output is connected to the piston input, creating the self-regulating feedback loop.

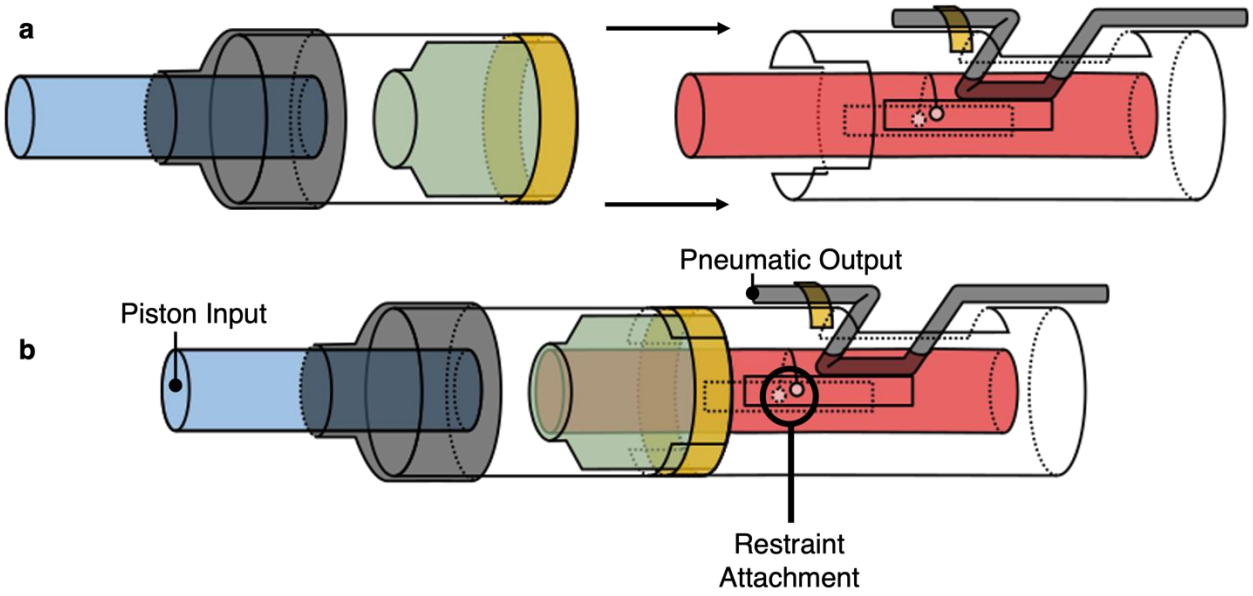

Figure S4. Regulator fabrication. (a) Schematic of piston and switch before attachment. (b) Schematic of the completed regulator. Materials are labeled in Figures S1-2.

5. SR Latch Fabrication

Fabricating an SR latch requires two pistons and a switch (Figure S1-2). The pistons are fastened on either end of the switch using tape (Matte Finish Magic Tape, Scotch), as shown in **Figure S5**.

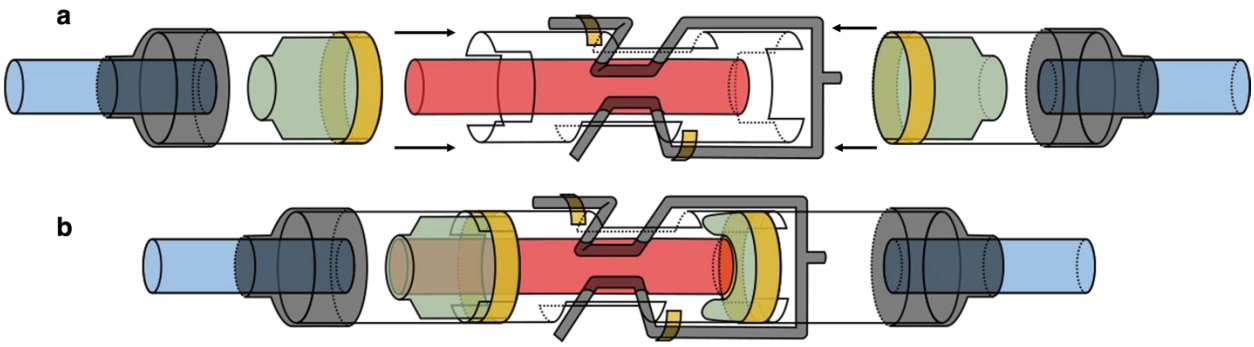

Figure S5. SR latch fabrication. (a) Schematic of pistons and switch before attachment. (b) Schematic of the completed SR latch. Materials are labeled in Figures S1-2. When one piston chamber is inflated, the inner switch inverts, changing the output of the latch. This state is maintained until the opposite switch is inflated (even if all pressure inputs are removed from the device), allowing one bit of nonvolatile memory to be stored.

6. Snap-Through Characterization

An isolated switch has three equilibria, each corresponding to a location where the piston tip exerts no force (**Figure S6**). These points shift position depending on the direction of travel of the switch due to system friction. The first and third equilibria are stable and correspond to the on and off states of the switch. Conversely, the second equilibrium is unstable, occurring in the middle of snap-through when forces from tube kinking act towards the right under a slight perturbation to the right (causing runaway in the right x-direction) and act towards the left under a slight perturbation to the left (causing runaway in the left x-direction). Perturbations in this state therefore cause the switch to snap to either the on or off positions, both of which are stable. Due to the two points of stable equilibrium, we call the isolated switch bistable. We note that the necessary snap-through force required to transition states is equal to the maximum (or minimum) force along force-distance curve between stable equilibria for forward (or backward) switching.

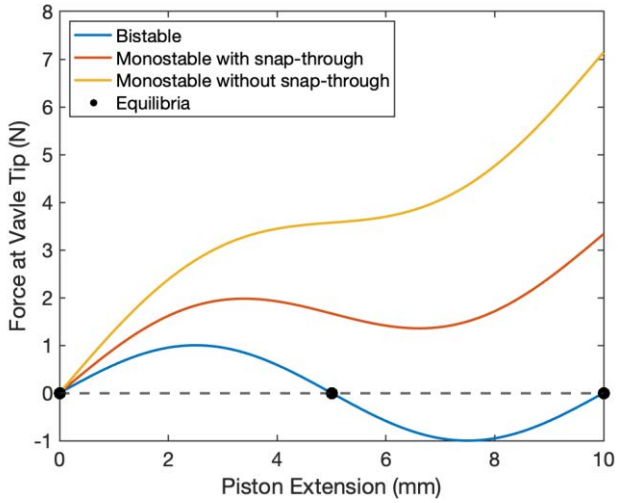

Figure S6. Snap-through characterization. Simulated force-displacement curves are displayed for clarity. See Figure S11 for measured force-displacement curves of the valve. Note that, for consistency with experimental measurements, a positive force value corresponds to an applied force in the negative x-direction (i.e., a positive tip force acts to push the switch towards the left). In practice, snap-through and stability characteristics can be tuned by choosing the elastic stiffness of restraints used in the valve.

Adding a rubber band to make a valve modifies the previous force distance curve, linearly increasing the force required to reach states in which the rubber band is extended (Figure S6). When large enough, this force removes the second two equilibria, converting the system to a monostable one. However, applying an external force (pressurizing the piston) still allows the system to enter "unstable" states, and causes the switch to turn on or off. Once again, the force required to reach a position on the force-distance curve is equal to the maximum force on the curve between those two positions on the displacement axis. The existence of a local maximum on the force-distance curve indicates that once that maximum force is reached, the switch rapidly snaps through. Consequently, the valve in this arrangement is monostable with snap-through.

Adding additional rubber bands further "stretches" the force distance curve vertically, increasing the force (and pressure) required to change switch states (Figure S6). Since extended states are affected by rubber bands to a greater degree, adding a sufficient quantity of rubber bands eliminates the local maximum in the force-distance curve. Although the valve no longer displays the same snap-through phenomenon, it still quickly changes states because the difference in force between on and off positions is small. If the valve is only subjected to binary high and low pressures, it still acts as a functional logic device. This system is referred to as monostable without snap-through.

7. IMPLY Gate Construction

An IMPLY gate is logically equivalent to a NOT gate leading to the first input of an OR gate; it outputs a Boolean 0 if and only if the two inputs are 1 and 0 respectively (**Figure S7**b). We construct an imply gate using a single valve by supplying a high pressure to the initially unkinked tube and treating the initially kinked tube and piston chamber as inputs (Figure S7c). A single-valve IMPLY gate decreases the size and complexity of logic circuits, because any system which contains a NOT gate leading to an OR gate can be immediately reduced (see **Figure S8**).

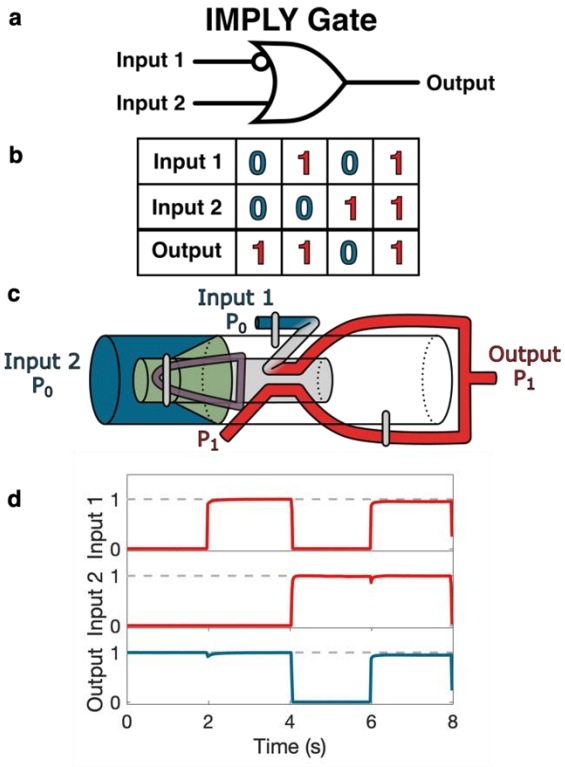

Figure S7. IMPLY gate construction. (a) Diagram representation of an IMPLY gate. (b) Truth table of an IMPLY gate. (c) Pneumatic connections required for a valve to behave as an IMPLY gate. (d) Experimental pneumatic input and output signals of an IMPLY gate.

8. XOR Gate Reduction

Exclusive OR (XOR) gates (a commonly used circuit block) output a Boolean 1 if exactly one of their inputs is a 1. To demonstrate the use of the IMPLY, INHIB, and unique 3-input gate inherent to this logic system, we show the minimum number of valves needed to construct a XOR circuit using different sets of logic gates. Using a set of NOT, AND, and OR (which previous soft logic systems provide), a XOR gate requires a minimum of five gates (Figure S8a-b). The addition of IMPLY and INHIB gates reduces the minimum number to three (Figure S8c). Finally, using the 3-input XOR* gate (Figure 3f), this number can be lowered to two (Figure S8d).

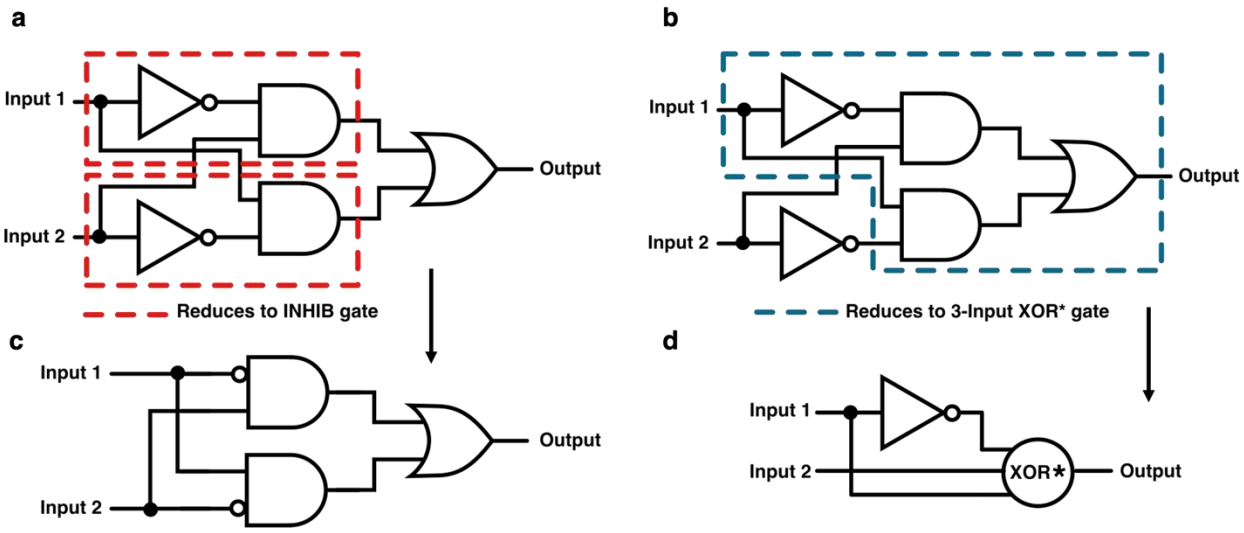

Figure S8. XOR gate reduction. (a-b) Minimum number of valves (five) required to fabricate a XOR gate from the set of AND, OR, and NOT. Possible gate reductions are outlined. (c) Minimum number of valves needed to fabricate a XOR gate with the addition of INHIB and IIMPLY gates (three valves). (d) Minimum number of valves needed to fabricate a XOR gate with the addition of the 3-input gate (two valves). We label this 3-input gate "XOR*" due to the ease of creating a XOR gate with it.

9. Modeling Snap-Through Pressure

Three component forces contribute to determining the pressure exerted on the internal membrane at which a valve snaps through: the switch snap-through force caused by tube kinking, the restoring force exerted by the elastic bands, and friction inherent to the system. Switch snap-through occurs when the force exerted on the piston head exceeds the sum of all of these components. To predict the force contribution of each component, we developed a semi-empirical model based on a combination of experimental and analytical techniques.

Tube-Kinking Force: Because tube kinking is difficult to accurately describe with a closed-form analytical model, we experimentally measured the force exerted by the tip of the switch as it transitions states using a universal testing machine (68SC-2, Instron). The maximum force recorded is considered the required snap-through force. We take the mean snap-forward and snap-backward forces across three valves to determine the snap-through forces and positions to be used in the model; snap-forward requires 0.5 N of force and occurs when the inner switch is displaced 1.3 mm with respect to the outer casing, while snap-backward also requires 0.5 N of force (applied in the opposite direction), but occurs at a displacement of 10.9 mm.

Elastic Stiffness: We modeled each set of elastic bands as an ideal spring, with stiffness coefficients determined experimentally. The force-displacement curves of different numbers of elastic bands (**Figure S9**b) were found using a universal testing machine (68SC-2, Instron). The slope of each curve is the calculated stiffness coefficient for that number of bands. It is desirable to calculate a length-independent property of the elastic material; we achieve this by multiplying each stiffness coefficient by the length of elastic material tested (7.62 cm).

Elastic Force: Due to the complex geometry of the valve, the elastic force applied to the piston tip cannot be described directly with Hooke's law. Instead, it is necessary to account for several system parameters. Critically, we assume there is a constant frictional "sticking" force (F_s) between the rubber band and edge of the outer switch chamber (Figure S9a). This sticking force separates the elastic into two sections with lengths L_1 and $L_2(x)$ respectively (note that the length L_1 is constant, while $L_2(x)$ varies with tip extension, x). If the difference in elastic tension between the two sides of this point, $|T_1(x) - T_2(x)|$, is less than F_s, then the amount of material in each section of elastic will remain constant. Otherwise, the elastic will slide until the difference in

tension is F_s. Other important parameters (shown in Figure S9a) are the distance between the inner piston and outer chamber (h), the initial horizontal distance between the sticking point and the rubber band (x_0), and the length-independent stiffness constant calculated previously (k_l). Additionally, we define $l_1(x)$ and $l_2(x)$ as the unstretched lengths of L_1 and $L_2(x)$ and d as extension of the elastic when the switch is retracted. Using this setup, it is possible to determine a set of analytically solvable equations for each state of the switch (sliding while extending, sliding

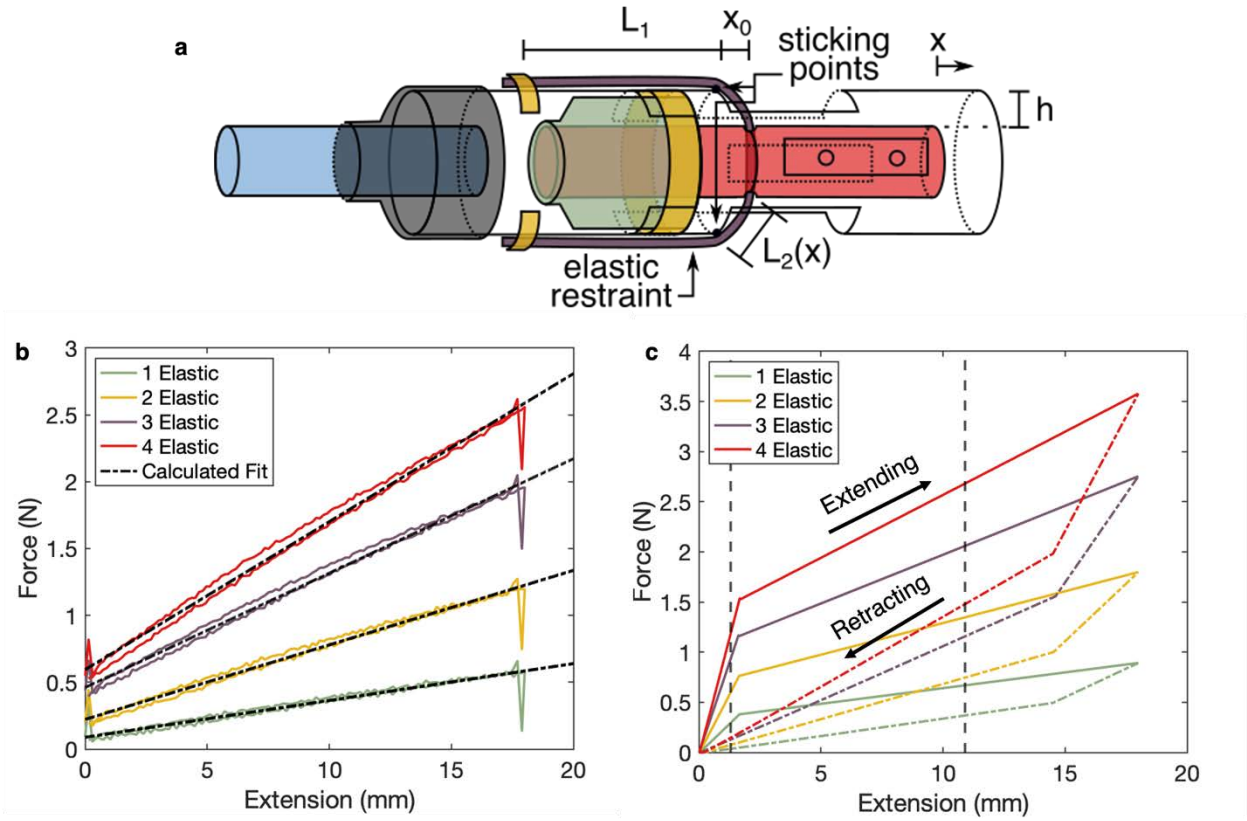

Figure S9. Elastic friction model. (a) Schematic illustrating variables used during modeling. Sharp deviations in force are artifacts from measurement. (b) Force of 1-4 elastic bands at different distances. Zero extension is set to be 7.62 cm of elastic band length. Stiffness constants cited in this work were found by taking the average slope of each data series. (c) Completed elastic force model output for a full cycle of extension and retraction. Elastic force values used to predict snap-through pressures were taken at 1.3 mm for extension and 10.9 mm for retraction (vertical lines).

while retracting, and the region where elastic sliding does not occur). The equations are solved iteratively while incrementally changing x, and using the results of the previous step to determine which state the switch is in. In this work, 4000 steps are used.

If the switch is sliding while extending (i.e. x is increasing, and $T_2(x) - T_1(x) \geq F_s$), we set the difference in tensions equal to F_s.

$$T_2(x) - T_1(x) = F_s \tag{1}$$

The tension in each section of elastic is a function of the stretched and unstretched lengths of that section, as well as the length independent stiffness constant.

$$T_1(x) = \frac{k_l}{l_1(x)}\big(L_1 - l_1(x)\big) \tag{2}$$

$$T_2(x) = \frac{k_l}{l_2(x)}\big(L_2(x) - l_2(x)\big) \tag{3}$$

The second stretched length of elastic is determined by extension.

$$L_2(x) = \sqrt{h^2 + (x + x_0)^2} \tag{4}$$

A final equation follows from the conservation of elastic material (assuming the portion of the elastic band inside the inner straw does not stretch).

$$l_1(x) + l_2(x) = L_1 + L_2(0) - d = L_1 - d + \sqrt{h^2 + {x_0}^2} \tag{5}$$

Equations 1-5 can be solved analytically to find the five unknown values: $T_1(x)$, $T_2(x)$, $l_1(x)$, $l_2(x)$, $L_2(x)$.

Specifically:

$$\begin{aligned} T_2(x) = \Bigg[& k_l L_1 - F_s d + k_l\sqrt{h^2 + (x + x_0)^2} + F_s L_1 + F_s\sqrt{h^2 + {x_0}^2} \\ & - \Big(k_l^2 L_1^2 + 2k_l^2 L_1\sqrt{h^2 + (x + x_0)^2} + k_l^2(h^2 + (x + x_0)^2) + 2k_l^2 F_s L_1^2 \\ & + 2k_l F_s L_1\sqrt{h^2 + {x_0}^2} - 2k_l F_s L_1\sqrt{h^2 + (x + x_0)^2} - 2k_l F_s L_1 d \\ & - 2k_l F_s\sqrt{(h^2 + (x + x_0)^2)(h^2 + {x_0}^2)} + 2k_l F_s d\sqrt{h^2 + (x + x_0)^2} \\ & + F_s^2 L_1^2 + 2F_s^2 L_1\sqrt{h^2 + {x_0}^2} - 2F_s^2 L_1 d + F_s^2(h^2 + {x_0}^2) \\ & - 2F_s^2 d\sqrt{h^2 + {x_0}^2} + F_s^2 d^2\Big)^{\frac{1}{2}} \Bigg] \frac{1}{2F_s} \end{aligned} \tag{6}$$

Finally, $T_{2x}(x)$, the component of $T_2(x)$ which acts in parallel to the piston, is easily found.

$$T_{2x}(x) = \frac{x + x_0}{L_2(x)}\, T_2(x) \tag{7}$$

If the switch is sliding while retracting (i.e. x is decreasing and $T_1(x) - T_2(x) \geq F_s$), the same process is followed, except Equation 1 must reflect the change in direction:

$$T_2(x) - T_1(x) = -F_s \tag{8}$$

Therefore, Equation 6 holds with the substitution $F_s \rightarrow -F_s$. Additionally, since the elastic band cannot support a compressive load, $T_1(x)$ and $T_2(x)$ are set as 0 if they are ever calculated as negative.

If the band is not sliding (i.e. $|T_2(x) - T_1(x)| \leq F_s$), the length $l_1(x)$ retains its value from the previous calculation step. Then $l_2(x)$ can be solved directly using Equation 5. The tension values $T_1(x)$, $T_2(x)$, and $T_{2x}(x)$ are then found with Equations 2,3,4 and 7.

To determine the force from the elastic band and friction felt by the piston, we run the algorithm described above, incrementing through two cycles of extension and retraction (each 18 mm in length) with the initial conditions $T_2(x) - T_1(x) = 0$ and $l_1(x) = L_1$. Using measured values from the valve, $L_1 = 60$ mm, $h = 2.5$ mm, $x_0 = 8$ mm. Additionally, k_l is 2.10, 4.24, 6.52, or 8.44 N for 1-4 elastic bands, respectively. Finally, F_s is a fitting parameter that varies with the number of elastics. For one elastic, we use $F_s = 0.2$ N. For more elastics, we multiply by the number of elastics used due to the increased force applied to the sticking point (e.g. for three elastics, $F_s = 0.6$ N). This value is reasonable, as it is on the same order of magnitude as the rest of the forces present in the system. We record $T_{2x}(x)$ at each step in the second cycle as the force experienced by the inner piston (Figure S9c). The final value for the elastic force ($F_{elastic}$) is taken from the second cycle, at the step with displacement equal to the snap-through or snap-back position (1.3 mm during extension for snap-through or 10.9 mm during retraction for snap-back).

Piston Force: The predicted piston force required to snap the switch through is determined by the component force balance described previously. **Figure S10**a and b show two experimental measurements demonstrating that the sum of components equals the device force total. If the

switch is snapping forward, the elastic force ($F_{elastic}$) and tube-kinking force (F_{tube}) oppose the piston force (F_{piston}).

$$F_{piston} = F_{elastic} + F_{tube} \tag{9}$$

If the switch is snapping back, F_{tube} and F_{piston} oppose $F_{elastic}$.

$$F_{piston} = F_{elastic} - F_{tube} \tag{10}$$

Piston Pressure: We experimentally determined a linear relationship to convert piston force (F_{piston}) to an equivalent input pressure (P). To determine this relationship, piston tip force was recorded at varying pressures (Figure S10c) using a universal testing machine (68SC-2, Instron), and two linear trendlines were fit (one during extension, and one during retraction).

During extension (with P given in kPa and F_{piston} in N):

$$P = \frac{F_{piston} + 0.157}{0.049} \tag{11}$$

During retraction:

$$P = \frac{F_{piston} - 0.140}{0.054} \tag{12}$$

The difference between extension and retraction is due to hysteresis caused by friction. The snap-through pressures predicted by this model are shown and compared to experimental results in Figure 2d.

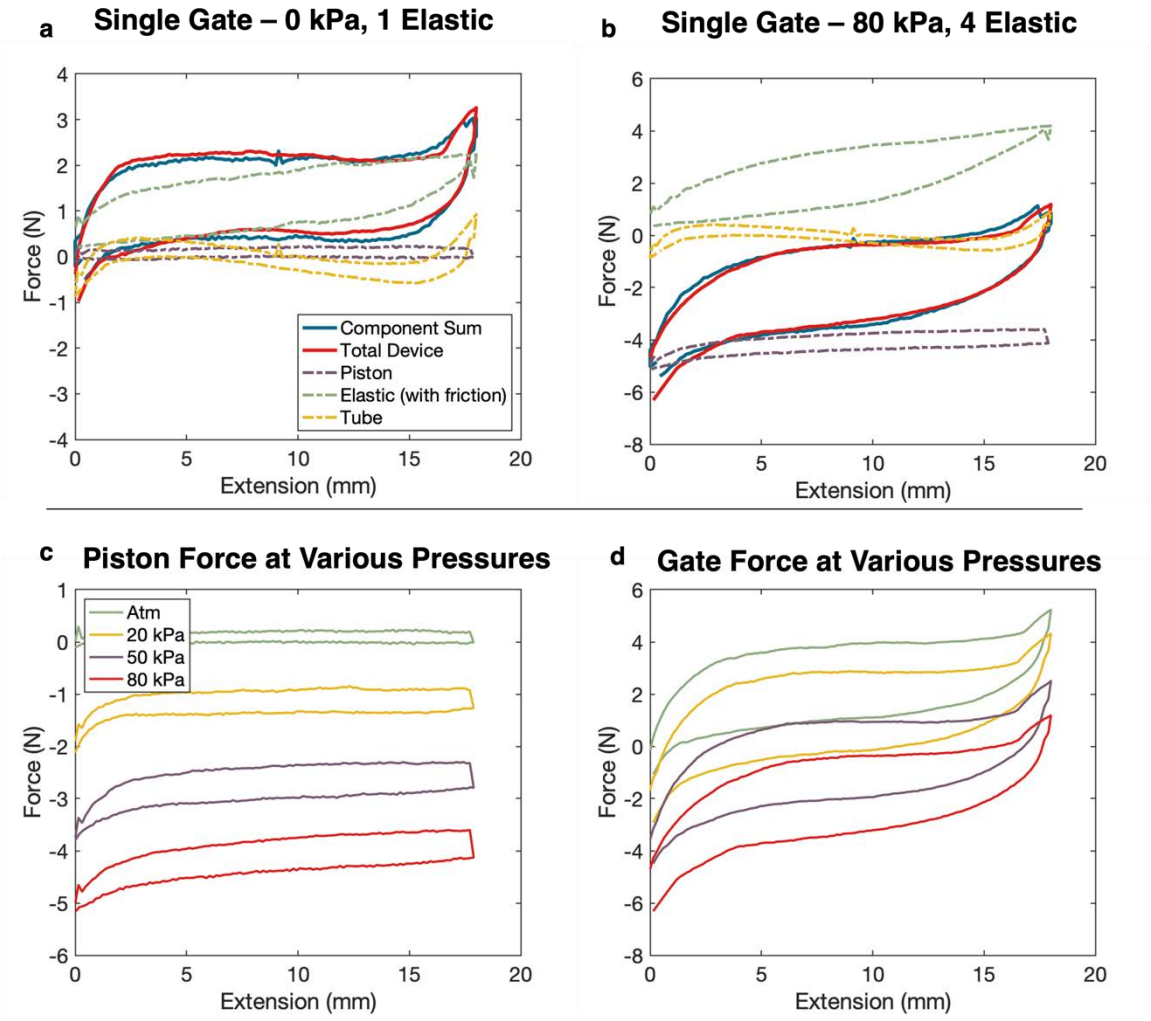

Figure S10. Force-distance measurements of gate components. (a-b) Force outputs of gate components (dashed) and the experimentally measured gate output at two different gate settings are depicted, showing good agreement between two component-based model (blue) and the actual measured force on the complete device (red). (c) Force output of the piston at different chamber pressures. Piston force is set to be negative as it opposes the force from elastic bands when configured as a gate. (d) Force output of the entire gate at different pressures (each with 4 elastic bands attached; legend shown in panel (c)).

10. Control Glove Fabrication

The control glove consists of five pressure regulators, fabricated as shown in Figure S4 The five regulators are secured to the forearm using two textile strips with hook-and-loop fasteners adhered to the ends (**Figure S11**a and Figure S11b). Each regulator input is connected to a common high-pressure line. The string restraint attached to each regulator interfaces with individual fingers by way of more hook-and-loop fasteners. One loop secures the string at the fingertip, while another loop—which holds a guiding tube—secures the string at the proximal phalanges (lower finger). Each string is connected to the regulator with an adjustable bend knot, which allows the string lengths to be adjusted without device refabrication.

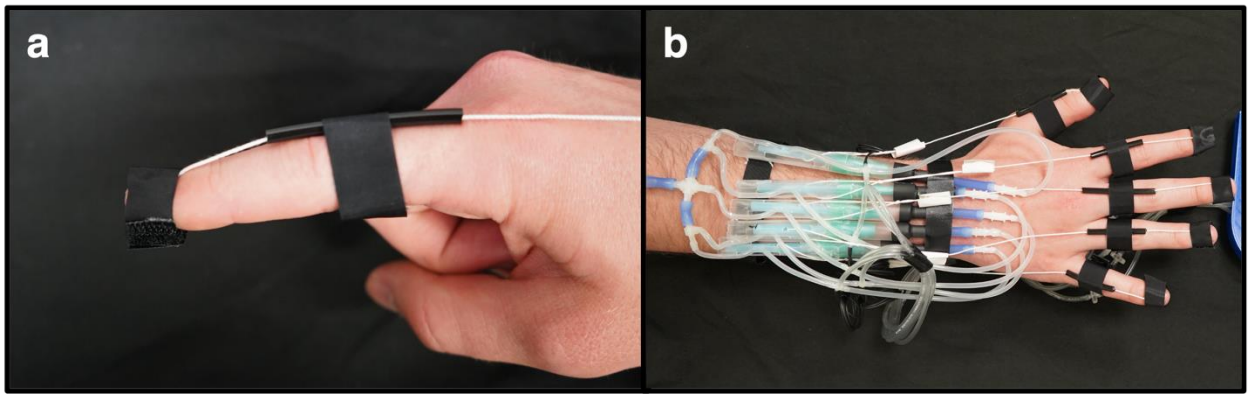

Figure S11. Images of the control glove. (a) Close-up image of the hook-and-loop fasteners used to secure string to finger. (b) Top view of the control glove on a human hand.

11. Soft Robotic Hand Fabrication

The robotic hand consists of 5 individual bending PneuNet actuators (**Figure S12**), fabricated as described by Mosadegh et al. (1). Silicone elastomer (Dragon Skin 30, Smooth-On) was used as the actuator material. The silicone mold is given in Data File S8 and S9. The housing for the actuators was 3D printed using a desktop printer (CR-10S Pro V2) with PLA (PLA+, eSUN) according to Data File S10 and S11. The two housing components (body and lid) were glued to each other (45198, Loctite). To interface with the control glove, the input of each finger actuator is connected to the output of a regulator. The output of each finger actuator is also connected to atmospheric pressure through a pneumatic pulldown resistor, i.e., 60cm of thin tubing.

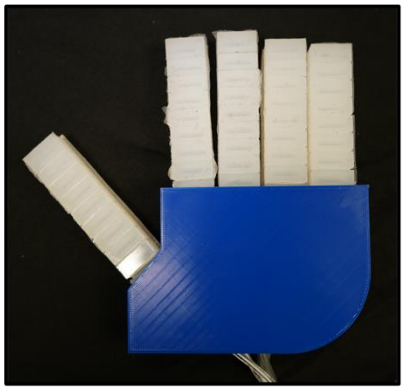

Figure S12. The complete control glove actuator.

12. Control Glove Finger Angle Matching

To demonstrate the utility of the control glove (and by extension, the analog regulator) as an intuitive human input for soft devices, we tune the control glove such that the finger angle of a user matches the actuator angle of the device. Using an embedded adjustable bend knot to modify the length of string connecting the regulator to a users' finger, we match the displacement response of the actuator to the finger. The results of this experiment are shown in Movie S2. Eight frames from the video were analyzed to determine the deviation between the actuator and finger angles (**Figure S13**a). We observed a maximum deviation of two degrees (Figure S13b).

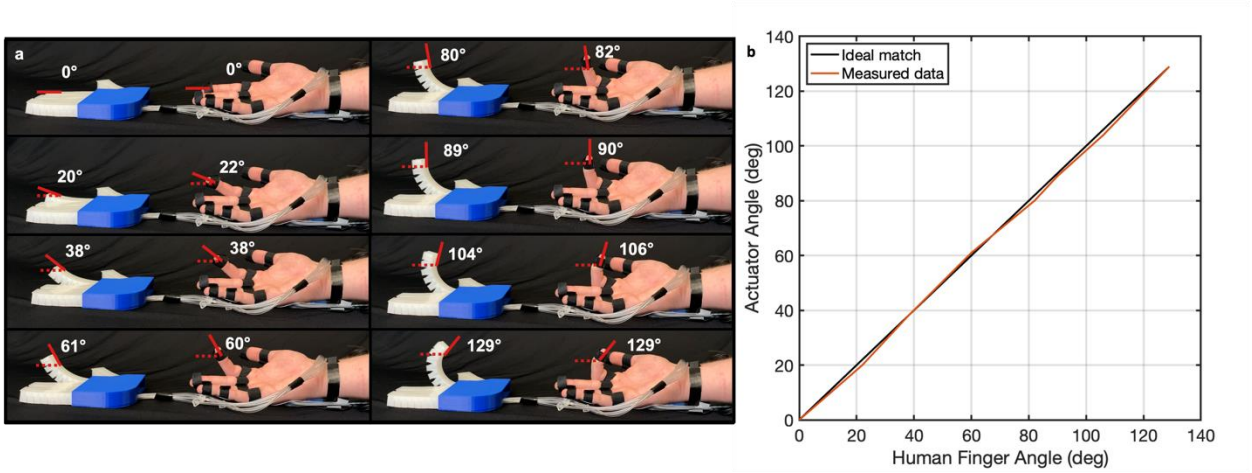

Figure S13. (a) Comparison of human and robotic finger angle from eight frames of Movie S2. (b) Graph of actuator angle and human finger angle compared to the ideal 1:1 response.

13. Combined Digital-Analog Circuits

Figure S14 displays an example circuit of a stable cascading counter using the gates available with our valves. Such a counter employs chained JK flip-flops, which are an extension of SR latches designed to avoid the possibility for an invalid input (where both the set and reset signals are high), accept a clock input, and toggle the output when both the J and K inputs are high and the clock input changes from low to high. Even with the reductions provided by INHIB gates, 30+ valves are required to physically construct the circuit. Functionally, this device would count the number of times the input switches from a pneumatic 0 to a pneumatic 1, up to a maximum of eight (i.e., binary "111"). Additional components would be necessary to enable a human user to program the circuit. This number of gates introduces many practical fabrication challenges, including compounded pneumatic resistance, actuation delays, and significant space requirements, making in impractical for use, especially on an untethered device. Instead, we develop a combined digital-analog circuit which can count an arbitrary number of cycles using just six physical valves.

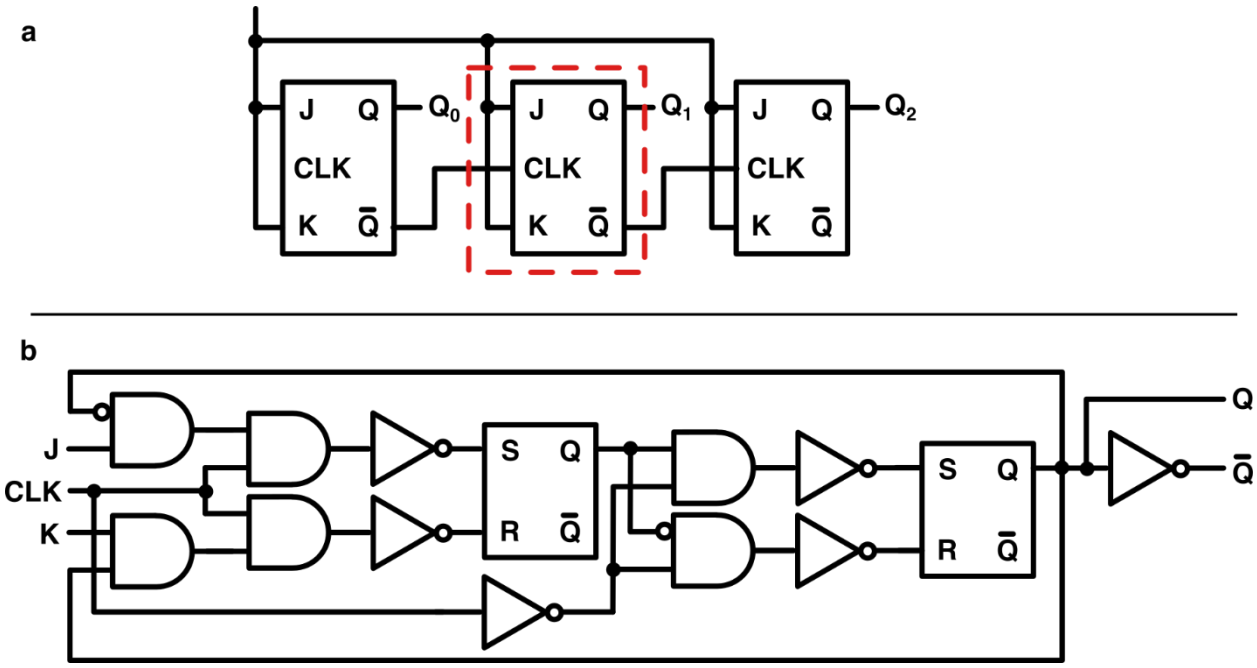

Figure S14. (a) A traditional cascading counter comprised of multiple JK-latches. (b) The logical diagram of a JK-latch comprised of gates that can be constructed with our valves.

14. Untethered Robot

The locomotive robot consists of three main components: a flexible frame, actuators (locomotive pistons and gripper), and the combined digital and analog logic control circuit. The frame consists of laser-cut straws assembled in a rectangular prism (**Figure S15**a). We laser cut holes in the straws for ease of construction (Data File S17**)**. Two different diameters of straws are used for construction (ST12100-Clear, Alink). Along the length of the frame, these two diameters slide freely within each other, allowing the frame to vary in length. Rubber bands restrain the frame to a minimum length when no opposing force is applied. On each of the four "legs" of the robot, low-friction fluorinated ethylene propylene sheets (3782, Fibre Glast) are affixed to enable sliding.

Piston actuators interface with the frame to symmetrically extend it when pressure is applied (Figure S15a). A modified PneuNet gripper is attached to the front of the robot (Figure S15a). The gripper allows the robot to retrieve objects and is molded with curable silicone (Dragon Skin 30, Smooth-On) with 3D printed molds (Data File S15 and S16). Piston actuators are also used to cyclically push a high-friction silicone (Dragon Skin 30, Smooth-On) foot into the ground (Figure

S15a) The silicone foot is also molded using 3D printed molds (Data File S13 and S14). Actuating one of the two feet during frame extension introduces an asymmetrical force that biases the robot to move in one direction. Robot motion can be controlled by switching which foot is actuated (Figure S15c).

The robot is pneumatically powered with a single onboard CO2 pressure vessel (17557, Fluval) regulated to a pressure of 138 kPa. This single, constant pressure is regulated to two separate lower levels using the soft analog regulators. The full control circuit is illustrated in Figure S15b. One pressure line runs to the PneuNet gripper, which requires a lower pressure compared to the piston actuators. A second pressure line runs to a regulator-controlled counter circuit that is designed to be set at the time of robot operation. A human user chooses how many rubber bands to tension on the regulator, thereby setting the robot counter. The main component of the logical control circuit is a central ring oscillator, which runs off of a third pressure line (at 138 kPa). The oscillator converts a constant pressure into an oscillating output, which enables robot locomotion. One output of the oscillator connects to the analog counter circuit through a pneumatic resistor and 80 cubic centimeter capacitor. Once the robot has walked for the pre-set number of steps, the pressure in the pneumatic capacitor will exceed the output of the human-set regulator, changing the output of the SR-latch from low-pressure to high pressure. Simultaneously, another output of the ring oscillator connects to the two pistons on the robot frame, as well as one of the silicone-foot pistons. The final oscillator output connects to the other silicone foot. During each oscillation cycle, the robot frame extends, and the silicone feet bias it to move forward (Figure S15c). Once the SR-latch in the timer circuit snaps through, the high-pressure output connects to three components in two steps. First, a pneumatic buffer switches on, allowing the down-regulated pressure line to actuate the PneuNet gripper. Second, two soft valves function as two-way relays and alternate which foot is connected to each section of the ring oscillator (thereby reversing the robot's direction). The robot will continue moving in the reversed direction until it is retrieved by a human user, or until the onboard pressure source is exhausted. The untethered robot was able to travel a total distance of at least 60 feet (over 50 body lengths) before depleting a single CO2 canister.

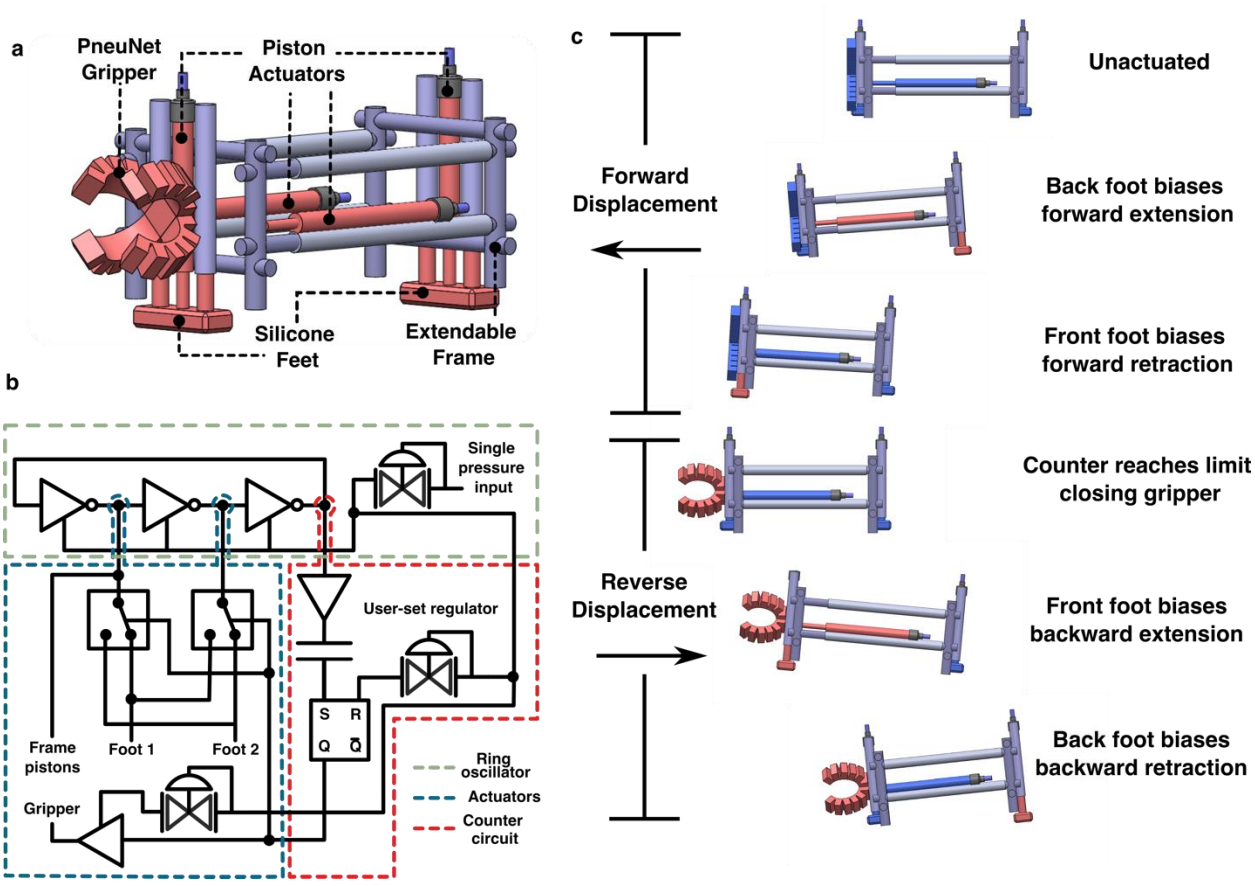

Figure S15. (a) Diagram of untethered robot frame and actuators. (b) Control circuit schematic of the soft robot. (c) Key robot modes during operation. The pressure source is a small metal tube of CO_2, with a steady pressure of 138 kPa which is then regulated by our analog valve.

15. Cushion Matrix Fabrication

The cushion matrix is fabricated in a similar manner to the rolling diaphragms; parchment paper (Heavy Duty Parchment, Katbite) is heat-pressed between two layers of heat-sealable textile. The parchment paper is patterned with a laser cutter (14000 Laser System, Epilog) at 30% power and 70% speed, using the vector file given in Data File S12. The heat-press (DK20SP, Geo Knight and Co Inc.) is activated 171 ℃ and 60 psi for 30 s. Excess textile and parchment paper are manually cut away, leaving six separate pouches. Each pouch has an input connection that tubing can be glued into.

16. Valve Failure Testing

The soft valve can fail in two critical ways: the soft diaphragm bursting, and pressure leaking through the kinked tubing. These two failure modes were tested individually across three valves. To test the breakthrough pressure of the kinked tube, input pressure was slowly increased until an increase in output pressure was measured with a pressure sensor (MGA-300-A-9V-R, SSI Technologies). The mean breakthrough pressure was 168 kPa. However, at the kink breakthrough pressure, the leaking flow rate is small. In cases where the output of the valve allows some amount of flow– such as when the valve is configured as a pressure regulator– this leakage may not impact performance. As input pressure increases past the breakthrough point, valve functionality will degrade.

To test the bursting pressure of the soft valve, piston input pressure was slowly increased until bursting was observed. The mean bursting pressure across three trials was 215 kPa. During these trials, the tube input was secured with an adhesive glue (45198, Loctite) in addition to heat shrink tubing (6363K213, McMaster-Carr) and (6363K214, McMaster-Carr). This modification is necessary to reach higher piston input pressures but does not otherwise change valve functionality.

Supporting Information References

1. B. Mosadegh, *et al.*, Pneumatic networks for soft robotics that actuate rapidly. *Adv. Funct. Mater.* **24**, 2163–2170 (2014).

Other supporting information for this manuscript includes:

Movie S1. Fabricating a valve. A video showing the valve fabrication process from start to finish.

Movie S2. Control glove operation. Top and side views of the control glove pressurizing individual actuators, holding actuator pressure in intermediate states, and rapidly pressurizing and depressurizing an actuator. Human finger angle is tuned to robotic finger angle.

Movie S3. Cushion matrix oscillation. A real-time video showing the external pressure distribution of the cushion matrix while the oscillation function is activated. Direct control of the cushion matrix with the analog control glove is shown.

Movie S4. Operation of untethered robot. Robot is programmed to travel to two different target distances and retrieves an object at each.

Movie S5. Valve repair process. A broken elastic band is replaced in one minute.

Movie S6. Valve to regulator conversion. Tubes are connected to a valve to configure it into a soft regulator.

Data file S1. Diaphragm vector. Dimensioned PDF file of the pattern used to laser cut the non-bonding layer needed during diaphragm fabrication.

Data file S2. Valve inner straw. Dimensioned PDF file of the pattern used to laser cut the inner straw used in a valve.

Data file S3. Valve outer straw. Dimensioned PDF file of the pattern used to laser cut the outer straw used in a valve.

Data file S4. Regulator inner straw. Dimensioned PDF file of the pattern used to laser cut the inner straw used in a regulator.

Data file S5. Regulator outer straw. Dimensioned PDF file of the pattern used to laser cut the outer straw used in a regulator.

Data file S6. SR latch inner straw. Dimensioned PDF file of the pattern used to laser cut the inner straw used in an SR latch.

Data file S7. SR latch outer straw. Dimensioned PDF file of the pattern used to laser cut the outer straw used in an SR latch.

Data file S8. Actuator mold base. Dimensioned PDF file of the base of the silicone mold used to cure elastomeric actuators.

Data file S9. Actuator mold top. Dimensioned PDF file of the top of the silicone mold used to cure elastomeric actuators.

Data file S10. Actuator housing body. Dimensioned PDF file of the body of the housing used to fabricate the control glove actuator.

Data file S11. Actuator housing lid. Dimensioned PDF file of the lid of the housing used to fabricate the control glove actuator.

Data file S12. Cushion matrix nonbonding layer. Dimensioned PDF file of the pattern used to laser cut the parchment-paper needed during cushion matrix fabrication.

Data file S13. Silicone foot mold 1. Dimensioned PDF file of half of the mold used to create the high-friction silicone foot for the untethered robot.

Data file S14. Silicone foot mold 2. Dimensioned PDF file of half of the mold used to create the high-friction silicone foot for the untethered robot.

Data file S15. Gripper base. Dimensioned PDF file of the base of the mold used to create the silicone gripper for the untethered robot.

Data file S16. Gripper top. Dimensioned PDF file of the top of the mold used to create the silicone gripper for the untethered robot.

Data file S17. Robot straws. Dimensioned PDF file the pattern used to laser cut straws for the untethered robot.